Modeling of wear in the Arlequin framework

Hachmi Ben Dhia, Mohamed Torkhani

Modeling of wear in the Arlequin framework

Hachmi Ben Dhia * and Torkhani Mohamed

Laboratoire MSS-Mat, Unité Mixte de Recherche 8579 CNRS
École Centrale Paris, Châtenay-Malabry 92295 cedex, France

SUMMARY

Wear phenomena are caused by interactions between contacting structures. The control of these phenomena is of great importance to predict the remaining lifetime of engineering or biological structures. In this paper, a precise mixed formulation for unilateral frictional contact problems involving wear, based upon the use of Archard's model, is developed. Classical Archard's model is shown to be nonlocal in the vicinity of the contact edges and this issue is addressed by carrying out delocalizing wear simulations. Moreover, a wear geometry update methodology is suggested to account for material removal due to wear. An extension, in the Arlequin framework, of the resulting wear simulation tool is suggested to model wear of thin structures submitted to the action of very localized contact loads. Finally, we suggest a strategy for multiscale and evolution-type contact problems (such as scratching of thin structures) by using a new concept of "Moving" Arlequin patch. Some numerical tests are carried out, showing the potential of our developments.

KEY WORDS: Fretting wear, unilateral contact, mixed formulation, thin structures, abrasion, scratching test, Arlequin method

1. INTRODUCTION

Fretting wear is a surface damage process caused by material removal as a consequence of small-amplitude cycling movement between two contacting bodies. These mechanisms are experienced in bolted-riveted joints [11, 12], shrink-fitted shafts [13], turbo machinery [14, 15], deep drawing [30], nuclear industry [37], human articulations/knee-joint protheses [31], etc... Nuclear industry for instance is interested in useful information for the prediction of the remaining lifetime of nuclear structures [28, 35, 36]. Information on the fretting wear s is of great importance for the design of future nuclear clusters and fuel rods.
When dealing with FE analysis of nonlinear contact problems [1, 2, 3, 4, 5, 10], it is of primary importance to use a precise and robust contact formulation that takes into account the wear depth to compute the contact forces. In 1994, Johansson [23] incorporates Archard's model in a FE contact algorithm within a penalized framework to evaluate the evolution of wear profiles and the inherent contact pressures under fretting regimes. Later, Stromberg [24] proposed an augmented lagrangian method all with a modified local form of Archard's model for FE wear analysis. Doing so, numerical difficulties such as parasitic oscillations of the discrete mechanical fields or algorithmic instabilities (see e.g. Podra [32]) are not circumvented. In this paper,

a continuous hybrid weak-strong *Characteristic-Set* field and placement based formulation, addressing the aforementioned issues, is used. In this formalism, unknown *Sign-like* fields are introduced to characterize the effective worn contact zone. Besides, the wear evolution law is given by Archard's model.

When studying contact wear modeling based on classical Archard's wear model, it is experienced that the concentration of contact forces near contact edges leads to a singular wear behaviour in this local zone [28] and that the use of the FEM gives rise to a mesh-dependency of the wear profile. Considering contact plastic deformations could be a physical based treatment (see e.g. [17, 41]). A phenomenological remedy is proposed in this paper and its stabilizing effect with respect to mesh size is highlighted.

The wear solutions in [23] and [24] did not take into consideration the wear-induced geometry change of the antagonist contact surfaces. In these works, wear is assumed to be small enough to have only a modest influence on the contact stress state. Then the use of initial contact geometries is justified. When wear amounts become significant, one cannot ignore the coupled evolution of wear and contact geometry. In fact, the wear profile evolution might change the contacting surface geometry and might also consequently change the contact stress distribution, which in turn impacts the wear depth rate *via* the wear model. Published works where contact geometry change caused by wear was accounted for are reported in [22, 29, 32, 33, 34, 38]. The strategy used therein precludes a geometry update that is achieved directly and incrementally, in a post-processing step, on the global mesh. The global mesh is incrementally updated after each loading cycle computation to take into account the calculated distribution of wear. Actually, the surface nodes are moved, in a post-processing stage, at a distance equal to the predicted nodal wear depths in the normal direction. For the next loading cycle, the finite element analysis is done on the new mesh, and so forth. This incremental global remeshing procedure ensures a successive improvement of the numerical solution, but is not efficient.

More recently, Paulin [41] and Madge [40] suggested partial mesh updates of a preselected local set of contact nodes, labeled "Wear Box" or "Wear Patch", respectively. This technique delimits the width of the contact region to be remeshed but the "Wear Patch" gluing to the global mesh is still a question of great practical and theoretical importance. In fact, gluing the local "Wear Patch" which geometry is updated to the global structure is still done using Multi-Point constraints. Thus, achieving conforming gluing requires very demanding matching meshes. This restrictive condition is not readily reachable for evolution-like contact problems. Moreover, the use of Lagrange junction forces leads to overconstraint and redundancy situations. Other more elaborated techniques such as XFEM [44, 45] or IEM [42, 46, 47] have been used to account for *Level-set* and Meshless-based description surface propagation, respectively. In this paper, a local geometry update methodology accounting for material loss is presented. Material removal is taken into account by means of local super-imposed refined Arlequin patchs that are geometrically-adapted to reflect the wear depth distribution. Gluing the local patchs is achieved in the Arlequin framework [7, 8, 9].

All these works have been dedicated to the wear behaviour prediction of mechanical solid components. Contact problems involving thin structures submitted to localized wear effects (sheet metal forming, stamping processes,...) have not received a great deal of attention in engineering and are summarily approached in mechanical literature. Some attempts in model situations are reported in [26, 25, 27]. Thin structures subjected to wear may experience contact loads that are so localized (contact edges, abrasive wear, cutting, scratching) that

their analysis by means of a classical thin structure FE model would be irrelevant. On the other side, a full three-dimensional analysis of such problems would be too costly. Owing to the Arlequin framework, we suggest to super-impose a local 3D FE model to a global thin structure one in the vicinity of the contact zone.
The outline of the paper is the following. Section 2 is devoted to the introduction of the mechanical wear problem and to the formulation of the virtual work principle for two contacting and wearing out bodies. The laws that define the frictional contact loads involving wear are given in section 3. The mixed Lagrangian formulation of the wear problem is then recalled in section 4. In section 5, some promising multiscale applications in numerical wear simulation are shown. More precisely, classical Archard's model is shown to be nonlocal in subsection 5.1 and delocalizing wear simulations are suggested to get rid of this numerical pathology. A geometry update procedure accounting for material loss due to wear is presented in subsection 5.3. Finally, the wear simulation tool is extended to encompass thin structures.

2. THE VIRTUAL WORK PRINCIPLE

2.1. Notations, hypotheses and problem definition

We consider the problem of frictional wear-contact between two deformable solids S^1 and S^2. The classical Lagrangian localization of these two contacting solids relies upon their respective reference configurations. Because of material removal due to wear, taking into account finite wear amounts requires a modification of the classical lagrangian formalism. Indeed, as represented in figure 1, the reference configurations of the worn solids become time-dependent. Let us notice $\Omega^1_{0,t}$ and $\Omega^2_{0,t}$ the (unknown) initial domains used to localize the worn solids at time t. Then, the current configurations of the solids S^1 and S^2 taking wear into consideration occupy the closures of the domains $\Omega^1_{t,t}$ and $\Omega^2_{t,t}$, defined, for each time t in the time interval $\boldsymbol{I} = [0, T]$ of study of the system, by the following deformation (or motion) application :

$$\begin{array}{c} \varphi^i_t : \Omega^i_{0,t} \rightarrow \Omega^i_{t,t} \\ \left(\boldsymbol{p}^i\right) \mapsto \varphi^i_t\left(\boldsymbol{p}^i\right) \end{array} \tag{1}$$

The boundary of each domain $\Omega^i_{0,t}$ is partitioned into parts Γ^i_u (assumed to be fixed) where the displacements are prescribed, $\Gamma^i_{g,t}$ where the surface loads are assumed to be given and $\Gamma^i_{c,t}$ the reference potential contact surface. The current positions of these boundary parts, denoted $\gamma^i_{u,t}$, $\gamma^i_{g,t}$ and $\gamma^i_{c,t}$ respectively, are assumed to constitute a partition of the boundary of $\Omega^i_{t,t}$.
In the reminder, the inertia terms will be neglected and the (fictive) time t will refer to increments of loading. Moreover, body and boundary classical forces are also neglected. Only contact loads will be considered.

2.2. Virtual Work Principle

Using classical notations [10], the Virtual Work Principle (VWP), combined with the action and reaction principle, reads : (for each fictive $0 \leq t \leq T$)
Find $\boldsymbol{u}(\mathrm{t}) = \left(\boldsymbol{u}^1(t), \boldsymbol{u}^2(t)\right) \in \boldsymbol{CA}_{u,t} = \boldsymbol{CA}^1_{u,t} \times \boldsymbol{CA}^2_{u,t}, \boldsymbol{R}(t) \in \mathbf{R} /\ \forall \boldsymbol{w} = \left(\boldsymbol{w}^1, \boldsymbol{w}^2\right) \in \boldsymbol{CA}_{u,t}$:

$$\mathbf{G}_{int}(\boldsymbol{u}(t), \boldsymbol{w}) = \mathbf{G}_c(\boldsymbol{R}, \boldsymbol{w}) \tag{2}$$

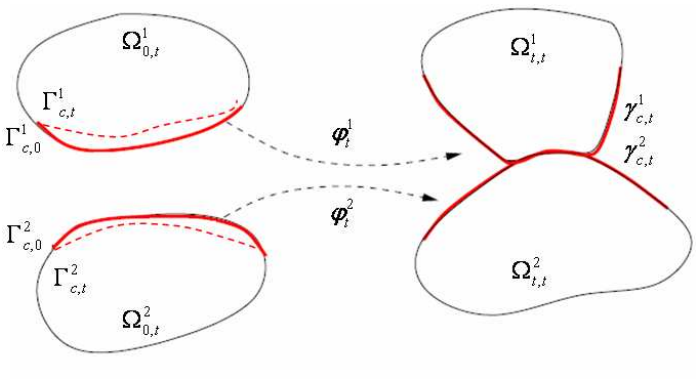

Figure 1. The contact/wear problem.

with :

$$\mathbf{G}_{int}(\boldsymbol{u}(t),\boldsymbol{w}) = \sum_{i=1}^{2} \mathbf{G}^i_{int} = \sum_{i=1}^{2} \int_{\Omega^i_{0,t}} Tr\left[\Pi^i\left(\boldsymbol{u}^i(t)\right)\left(\nabla \boldsymbol{w}^i\right)^T\right] d\Omega^i_{0,t} \tag{3}$$

$$\mathbf{G}_c(\boldsymbol{R},\boldsymbol{w}) = \int_{\Gamma_{c,t}} \boldsymbol{R}.\left[\!\left[\boldsymbol{w}\right]\!\right] d\Gamma \tag{4}$$

In system (2), $\left(\boldsymbol{CA}^i_{u,t}\right)_{i=1,2}$ denote the spaces of kinematically admissible fields defined in $\Omega^i_{0,t}$, $\boldsymbol{u}^i$ the displacement field, $\Gamma_{c,t}\left(=\Gamma^1_{c,t}\right)$ is the potential "slave" and reference contact surface, Π^i is the first Piola-Kirchhoff stress tensor defined in $\Omega^i_{0,t}$ and $\boldsymbol{R} = \boldsymbol{R}^1(\boldsymbol{p},t) = -\boldsymbol{R}^2(\overline{\boldsymbol{p}},t)$ the nominal vector-valued unknown density of contact forces experienced in $\Gamma_{c,t}$ by the worn solid S^1 from the worn solid S^2 where $\bar{\boldsymbol{p}}$ is the point belonging to the "master" surface $\Gamma^2_{c,t}$ paired with the point $\boldsymbol{p}$ of the "slave" surface $\Gamma^1_{c,t}$ by using the classical proximity procedure [6]. The reference pairing application A^1_p is defined as follows :

$$\begin{array}{c} A^1_p : \Gamma^1_{c,t} \to \Gamma^2_{c,t} \\ \left(\boldsymbol{p}^1\right) \mapsto \overline{\boldsymbol{p}}^1(t) \end{array} \tag{5}$$

Moreover, $\forall \boldsymbol{p}^1 \in \Gamma_{c,t}, \left[\!\left[\boldsymbol{w}\right]\!\right]\left(\boldsymbol{p}^1\right) = \boldsymbol{w}^1\left(\boldsymbol{p}^1\right) - \boldsymbol{w}^2\left(A^1_p\left(\overline{\boldsymbol{p}}^1,t\right)\right)$ is the jump-like field defined on $\Gamma_{c,t}$.

System (2) has to be supplemented with material behaviour laws, initial conditions, and wear and contact laws. For the sake of simplicity, an hyperelastic behaviour is assumed for the constitutive materials of the solids S^1 and S^2. That is :

$$\Pi^i = \rho^i_0 \frac{\partial W^i(\mathbb{F}^i)}{\partial \mathbb{F}^i} \tag{6}$$

where W^i is a local internal elastic energy per mass unit and $\mathbb{F}^i$ is the deformation gradient tensor. The solids are assumed to be initially free of residual stresses. As initial condition, we take :

$$\boldsymbol{u}^i(\cdot,0) = \boldsymbol{u}^{i0} = 0, \in \Omega_{0,0} \tag{7}$$

The contact interface model taking wear into account constitutes the subject of the next section.

3. CONTACT LAWS TAKING WEAR INTO ACCOUNT

3.1. Archard's wear model

In a fretting process, wear removes volume. To simulate this material loss mechanism, Archard [16] suggested a model which is written in terms of wear volume loss. Mc Coll [38] adapted this global model by introducing a wear depth variable, denoted w_n, the mean rate of which characterizing the evolution of the contacting surfaces in the normal direction. In our considered framework, we assume that the evolution of wear pulled-back to the reference configuration is given by the following generalized Archard's-like evolution law :

$$\left| \begin{array}{l} \frac{dw_n^i(\boldsymbol{p},t)}{dt} = C^i \lambda(\boldsymbol{p},t) \left\| [\![\boldsymbol{v}_\tau(\boldsymbol{p},t)]\!] \right\| \\ w_n^i(\boldsymbol{p},0) = 0 \ \forall \boldsymbol{p} \in \Gamma_{c,t}^i \end{array} \right. \tag{8}$$

where $[\![\boldsymbol{v}_\tau]\!]$ refers to the relative sliding velocity, λ is the nominal contact pressure and C^i are wear coefficients providing agreement between theory and experiment [34, 32].
Observe that the evolution of reference wear depth is on $\Gamma_{c,t}$. Let's define the current infinitesimal variation of wear as following :

$$\delta_x w^t = C \lambda_x \left\| [\![\boldsymbol{v}_\tau]\!] \right\| \tag{9}$$

Let's denote $\delta_x S^t$ and $\delta_p S$ the infinitesimal surfaces in the current and reference configurations, respectively. Since the Archard's model invloves only wear evolution in the normal direction, the infinitesimal worn volume is defined by $\delta_x V^w = \delta_x S^t \times \delta_x w^t$. A basic hypothesis lying behind a wear model is to stipulate that the worn volume is conserved. Then, the reference infinitesimal wear variation is defined by $\delta_p w = \delta_x w^t$ ($\delta_p S = \delta_x S^t$) and $\frac{\delta_x S^t}{\delta_p S} \delta_x w^t$ for small and large perturbations, respectively. From equation 9, from the definition of the nominal contact pressure $\lambda_p = \lambda_x \frac{\delta_x S^t}{\delta_p S}$ and from the objectivity of the relative tangential velocity $[\![\boldsymbol{v}_\tau]\!]$, it comes that :

$$\delta_p w = C \lambda_p \left\| [\![\boldsymbol{v}_\tau]\!] \right\| \tag{10}$$

These relations ensure the well-posedness of the suggested wear model.
Equation 8 is written in the following incremental form :

$$\left| \begin{array}{l} \frac{\Delta w_n^i(\boldsymbol{p},t)}{\Delta t} = C^i \lambda(\boldsymbol{p},t) \left\| [\![\frac{\boldsymbol{u}_\tau(\boldsymbol{p},t)}{\Delta t}]\!] \right\| \\ w_n^i(\boldsymbol{p},0) = 0 \ \forall \boldsymbol{p} \in \Gamma_{c,t}^i \end{array} \right. \tag{11}$$

3.2. The Characteristic-Set based Signorini unilateral wear model

Contact fields are defined by means of *Signorini* and *Coulomb* interface models. One of our formulation key points is the equivalent setting of the latter in terms of equations *via* the use of unknown Sign-like fields, defined on the assumed to be known potential contact surfaces [6, 10].
Let's define the current worn positions $\boldsymbol{x}_1^w$ and $\boldsymbol{x}_2^w$ of a point $\boldsymbol{p} \in \Gamma_{c,t}$ and the corresponding paired point $\overline{\boldsymbol{p}}$ as follows :

$$\boldsymbol{x}_1^w = \varphi_t^1 (\boldsymbol{p}, t) \tag{12}$$

$$\boldsymbol{x}_2^w = \varphi_t^2 (\overline{\boldsymbol{p}}, t) \tag{13}$$

where $\boldsymbol{n}_t = -\boldsymbol{n}_t^2\left(\boldsymbol{x}_2^w\right)$ is the unit inward normal to the solid S^2 at $\boldsymbol{x}_2^w$.
The classical *Signorini* contact laws modified to account for wear phenomena read :

$$\left(\boldsymbol{x}_1^w(\boldsymbol{p},t) - \boldsymbol{x}_2^w(\overline{\boldsymbol{p}},t)\right)\cdot\boldsymbol{n}_t \leq 0 \qquad \text{for } (\boldsymbol{p},t)\in\Gamma_{c,t}\times \mathrm{I} \tag{14}$$

$$\lambda(\boldsymbol{p},t) \leq 0 \qquad \text{for } (\boldsymbol{p},t)\in\Gamma_{c,t}\times \mathrm{I} \tag{15}$$

$$\lambda(\boldsymbol{p},t)\left(\boldsymbol{x}_1^w(\boldsymbol{p},t) - \boldsymbol{x}_2^w(\overline{\boldsymbol{p}},t)\right)\cdot\boldsymbol{n}_t = 0 \qquad \text{for } (\boldsymbol{p},t)\in\Gamma_{c,t}\times \mathrm{I} \tag{16}$$

Using the definitions (12-13) in (14-16) gives :

$$d_n^w(\boldsymbol{p},t) \leq 0 \qquad \text{for } (\boldsymbol{p},t)\in\Gamma_{c,t}\times \mathrm{I} \tag{17}$$

$$\lambda(\boldsymbol{p},t) \leq 0 \qquad \text{for } (\boldsymbol{p},t)\in\Gamma_{c,t}\times \mathrm{I} \tag{18}$$

$$d_n^w(\boldsymbol{p},t)\lambda(\boldsymbol{p},t) = 0 \qquad \text{for } (\boldsymbol{p},t)\in\Gamma_{c,t}\times \mathrm{I} \tag{19}$$

By using a Sign-like function, what can be called the *Signorini* contact laws taking into account wear, (17-19), are transformed into the following multi-valued equalities :

$$\lambda = S_u^w\left(\lambda - \rho_n d_n^w\right) \tag{20}$$

$$S_u^w = 1_{\mathbb{R}^-}\left(\lambda - \rho_n d_n^w\right) \tag{21}$$

with 1_{K} denotes the characteristic function of the set K and ρ_n is a strictly positive real parameter.

3.3. The Characteristic-Set based Coulomb frictional wear model

As mentioned in [10], *Coulomb* friction laws can be equivalently written by introducing the *Characteristic-Set* field S_f as follows :

$$(1 - S_u^w)\boldsymbol{\Lambda} = 0 \tag{22}$$

$$\boldsymbol{R_\tau} = \mu S_u^w \lambda \boldsymbol{\Lambda} \tag{23}$$

$$\boldsymbol{\Lambda} = S_f\boldsymbol{\Lambda} + (1 - S_f)\left(\frac{\boldsymbol{\Lambda} + \rho_\tau[\![\boldsymbol{v}_\tau]\!]}{||\boldsymbol{\Lambda} + \rho_\tau[\![\boldsymbol{v}_\tau]\!]||}\right) \tag{24}$$

$$S_f = 1_{B(0,1)}\left(\boldsymbol{\Lambda} + \rho_\tau[\![\boldsymbol{v}_\tau]\!]\right) \tag{25}$$

where S_u^w is defined by (21), μ is the friction coefficient, ρ_τ is a strictly positive real parameter and $B(0,1)$ is the unit ball of $\mathbb{R}^d$ $(d = 2, 3)$.

4. MIXED CONTINUOUS FORMULATION OF THE WEAR PROBLEM

By using (2-4), (20-21) and (22-25), a weak-strong hybrid formulation of the problem described above can be derived by following in essence the lines given in [10] and [6]. It reads :
Find $\left(\boldsymbol{u}, \lambda, \boldsymbol{\Lambda}, w_n^i, S_u^w, S_f\right) \in \boldsymbol{CA}_u \times H_c \times \boldsymbol{H}_f \times H_w \times L^\infty\left(\Gamma_{c,0}; \{0,1\}\right)^2 / \ \forall\left(\boldsymbol{w}^i, \lambda^*, \Lambda^*\right)$,

- *Virtual Work Principle*

$$\begin{aligned}&\sum_{i=1}^{2} G_{int}^i\left(\boldsymbol{u}^i, \boldsymbol{w}^i\right) - \int_{\Gamma_{c,t}} S_u^w \lambda[\![\boldsymbol{w}_n]\!]d\Gamma \\ &\quad - \int_{\Gamma_{c,t}} \mu S_u^w \lambda\left[S_f\Lambda + (1 - S_f)\,\frac{\Lambda + \rho_\tau[\![\boldsymbol{v}_\tau]\!]}{\|\Lambda + \rho_\tau[\![\boldsymbol{v}_\tau]\!]\|}\right][\![\boldsymbol{w}_\tau]\!]d\Gamma = 0\end{aligned} \tag{26}$$

- *Signorini-Archard weak law*

$$-\frac{1}{\rho_n}\int_{\Gamma_{c,t}}\left[\lambda-S_u^w\left(\lambda-\rho_n d_n^w\right)\right]\lambda^* d\Gamma=0 \tag{27}$$

- *Coulomb weak law*

$$\begin{aligned}\frac{1}{\rho_\tau}\int_{\Gamma_{c,t}}\mu S_u^w\lambda\left\{\Lambda-\left[S_f\left(\Lambda+\rho_\tau[\![\boldsymbol{v}_\tau]\!]\right)+\left(1-S_f\right)\frac{\Lambda+\rho_\tau[\![\boldsymbol{v}_\tau]\!]}{\|\Lambda+\rho_\tau[\![\boldsymbol{v}_\tau]\!]\|}\right]\right\}\Lambda^* d\Gamma\\ +\int_{\Gamma_{c,t}}\left(1-S_u^w\right)\Lambda\Lambda^* d\Gamma=0\end{aligned} \tag{28}$$

- *Sign-like fields*

$$S_u^w=1_{\mathbb{R}^-}\left(\lambda-\rho_n d_n^w\right) \tag{29}$$

$$S_f=1_{B(0,1)}\left(\boldsymbol{\Lambda}+\rho_\tau[\![\boldsymbol{v}_\tau]\!]\right) \tag{30}$$

- *Archard's type local wear law*

$$\frac{dw_n^i}{dt}(.,t)=C^i\lambda(.,t)\left\|[\![\boldsymbol{v}_\tau(.,t)]\!]\right\|,\ i\in 1,2 \tag{31}$$

- *Initial conditions*

$$\boldsymbol{u}^i(.,0)=0 \text{ in } \Omega_{0,0}^i \tag{32}$$

$$w_n^i(.,0)=0 \text{ in } \Gamma_{c,0} \tag{33}$$

where :

- G_{int}^i is defined by (3),
- $\boldsymbol{CA}_{u,t}$, H_c, $\boldsymbol{H}_f$ and H_w are the space of kinematically admissible displacement field, the space of contact Lagrange multipliers, the space of friction (semi-) Lagrange multipliers and the space of the wear field, respectively.

To derive an incremental form of (26-33), we consider the interval of study $\boldsymbol{I}=[0,T]$ to be a collection of non-overlapping sub-intervals $[t_k,t_{k+1}]$, *i.e.*, $\boldsymbol{I}=\bigcup_{k=0}^{n_T}[t_k,t_{k+1}]$. We denote by $\Delta t_k=t_{k+1}-t_k=\Delta t$ the time step (chosen here to be constant for simplicity) and by $\boldsymbol{u}_k=\left(\boldsymbol{u}_k^1,\boldsymbol{u}_k^2\right)$ the discrete approximation of the field $\boldsymbol{u}(t_k)$ at time $t=t_k$ and by $w_{nk}=\left(w_{nk}^1,w_{nk}^2\right)$ the approximation of $w_n(t_k)$.
Assuming that the fields $\left(\boldsymbol{u}_{k-1},\lambda_{k-1},\boldsymbol{\Lambda}_{k-1},w_{n(k-1)},S_{u(k-1)}^w,S_{f(k-1)}\right)$ are known, we solve the following problem:
Find $(\boldsymbol{u}_k,\lambda_k,\boldsymbol{\Lambda}_k,w_{nk},S_{uk}^w,S_{fk})\in\boldsymbol{CA}_u\times H_{c,t}\times\boldsymbol{H}_{f,t}\times H_{w,t}\times L^\infty(\Gamma_{c,t};\{0,1\})^2$;

$$\mathbf{G}_{int}(\boldsymbol{u}_k,\boldsymbol{w})+\mathbf{G}_{cont}(\lambda_k,\boldsymbol{u}_k,\boldsymbol{w})+\mathbf{G}_{fric}(\boldsymbol{\Lambda}_k,\lambda_k,\boldsymbol{u}_k,\boldsymbol{w})=0,\qquad\forall\boldsymbol{w}\in\boldsymbol{CA}_u \tag{34}$$

$$\mathbf{G}_{cont}^{weak}(\lambda_k,\boldsymbol{u}_k,\lambda^*)=0,\qquad\forall\lambda^*\in H_{c,t} \tag{35}$$

$$\mathbf{G}_{fric}^{weak}(\boldsymbol{\Lambda}_k,\lambda_k,\boldsymbol{u}_k,\boldsymbol{\Lambda}^*)=0,\qquad\forall\boldsymbol{\Lambda}^*\in\boldsymbol{H}_{f,t} \tag{36}$$

with :

$$\mathbf{G}_{int}\left(\boldsymbol{u}_k,\boldsymbol{w}\right)=\sum_{i=1}^{2}\int_{\Omega_{0,t}^{i}}Tr\left[\Pi_k^i\left(\nabla\boldsymbol{w}^i\right)^T\right]d\Omega_{0,0}^i \tag{37}$$

$$\mathbf{G}_{cont}\left(\lambda_k,\boldsymbol{u}_k,\boldsymbol{w}\right)=-\int_{\Gamma_{c,t}}S_{uk}^w g_{nk}^w[\![\boldsymbol{w}_n]\!]d\Gamma \tag{38}$$

$$\mathbf{G}_{fric}\left(\Lambda_k,\lambda_k,\boldsymbol{u}_k,\boldsymbol{w}\right)=-\int_{\Gamma_{c,t}}\mu S_{uk}^w\lambda_k\left\{S_{fk}\boldsymbol{\Lambda}_k+\left(1-S_{fk}\right)\frac{\boldsymbol{g}_{\tau k}}{\|\boldsymbol{g}_{\tau k}\|}\right\}\cdot[\![\boldsymbol{w}_\tau]\!]d\Gamma \tag{39}$$

$$\mathbf{G}_{cont}^{weak}\left(\lambda_k,\boldsymbol{u}_k,\lambda^*\right)=\int_{\Gamma_{c,t}}-\frac{1}{\rho_n}\left\{\lambda_k-S_{uk}^w g_{nk}^w\right\}\lambda^* d\Gamma \tag{40}$$

$$\begin{aligned}\mathbf{G}_{fric}^{weak}\left(\Lambda_k,\lambda_k,\boldsymbol{u}_k,\Lambda^*\right)=\int_{\Gamma_{c,t}}\frac{-\mu S_{uk}^w\lambda_k}{\underline{\rho}_\tau}\{\boldsymbol{\Lambda}_k-\left(S_{fk}\boldsymbol{\Lambda}_k+\left(1-S_{fk}\right)\frac{\boldsymbol{g}_{\tau k}}{\|\boldsymbol{g}_{\tau k}\|}\right)\}\boldsymbol{\Lambda}^* d\Gamma+\\ \int_{\Gamma_{c,t}}\left(S_{uk}^w-1\right)\boldsymbol{\Lambda}_k\boldsymbol{\Lambda}^* d\Gamma=0\end{aligned} \tag{41}$$

where :

$$\begin{aligned}&\Pi_k^i=\Pi^i\left(\boldsymbol{u}_k^i\right)\\&g_{nk}^w=\lambda_k-\rho_n d_{nk}^w\\&d_{nk}^w=[\![\boldsymbol{x}_k]\!]\cdot\boldsymbol{n}_k-\sum_{i=1}^{2}w_{nk}^i\\&[\![\Delta\boldsymbol{u}_{\tau k}]\!]=\Delta\boldsymbol{u}_{\tau k}-\Delta\boldsymbol{u}_{\tau(k-1)}\\&w_{nk}^i=w_{n(k-1)}^i+C^i\lambda_k\left\|[\![\Delta\boldsymbol{u}_{\tau k}]\!]\right\|\\&S_{uk}^w=1_{\mathbb{R}^-}\left(g_{nk}^w\right)\\&\boldsymbol{g}_{\tau k}=\Lambda_k+\underline{\rho}_\tau[\![\Delta\boldsymbol{u}_{\tau k}]\!]\\&S_{fk}=1_{B(0,1)}\left(\boldsymbol{g}_{\tau k}\right)\\&\underline{\rho}_\tau>0\end{aligned}$$

Using the FEM, a straightforward hybrid discrete formulation of the continuous incremental problem (34-41) can be obtained.

4.1. An incremental numerical simulation staregy

The numerical approximation of the mechanical problem (34-41) supposes that the potential worn contact surface $\Gamma_{c,t}$ must be adapted continuously within the solution strategy. Moreove, baring the computational constraints in mind, it will not be efficient to simulate individually and explicitly all the fretting cycles.
To address these two numerical challenges, we suggest a (seemingly) new incremental wear formulation, based on a technique which is similar to the "cycle jumping technique", described by Ding and Col. in [39] :

1. If wear is not so high over a fixed number of cycles k^i (depending on the wear kinetics), one can carry out the corresponding "wear geometry step" $\Delta\tau^i=k^i\times\Delta t, k^i\geq 1$ on a frozen contact geometry Γ_{c,k^i}. For a point $\boldsymbol{p}$ of the fixed contact surface Γ_{c,k^i} :

$$\left|\begin{aligned}\boldsymbol{x}_1^w&=\varphi^1\left(\boldsymbol{p},t\right)-\boldsymbol{w}_n^1\left(\boldsymbol{p},t\right)\boldsymbol{n}_{k^i}\\\boldsymbol{x}_2^w&=\varphi^2\left(\overline{\boldsymbol{p}},t\right)+\boldsymbol{w}_n^2\left(\overline{\boldsymbol{p}},t\right)\boldsymbol{n}_{k^i}\end{aligned}\right. \tag{42}$$

Then, equations (14-16), pulled-back to the reference contact surface Γ_{c,k^i}, read :

$$(\boldsymbol{x}_1^w(\boldsymbol{p},t) - \boldsymbol{x}_2^w(\overline{\boldsymbol{p}},t)) \cdot \boldsymbol{n}_{k^i} \leq 0 \qquad \text{for } (\boldsymbol{p},t) \in \Gamma_{c,k^i} \times \mathrm{I} \tag{43}$$

$$\lambda(\boldsymbol{p},t) \leq 0 \qquad \text{for } (\boldsymbol{p},t) \in \Gamma_{c,k^i} \times \mathrm{I} \tag{44}$$

$$\lambda(\boldsymbol{p},t)\,(\boldsymbol{x}_1^w(\boldsymbol{p},t) - \boldsymbol{x}_2^w(\overline{\boldsymbol{p}},t)) \cdot \boldsymbol{n}_{k^i} = 0 \qquad \text{for } (\boldsymbol{p},t) \in \Gamma_{c,k^i} \times \mathrm{I} \tag{45}$$

Before changing the contact geometry Γ_{c,k^i}, the contact gap, modified to take into account the wear kinematics, is defined as follows :

$$\boldsymbol{d}_n^w = (\boldsymbol{x}_1^w - \boldsymbol{x}_2^w) = \left(d_n - (\boldsymbol{w}_n^1 + \boldsymbol{w}_n^2)\right) \boldsymbol{n}_{k^i} \tag{46}$$

2. The contact geometry is updated only at the end of each "wear geometry step" and not before. For a given contact geometry and wear kinetics, an optimum choice could be found, for example, by carrying out parametric investigations. The same operations as in **1** are achieved on the contact surface $\Gamma_{c,k^{i+1}}$.

The procedure is the following :

i. achieve the numerical simulation on the initial given contact geometry $\Gamma_{c,0} = \Gamma_{c,k^0}$;
ii. calculate the corresponding nodal wear depths for the first "wear geometry step", ie for a number of cyles N^0, corresponding to the simulation time $\Delta\tau^0 = k^0 \times \Delta t$;
iii. update the contact geometry by the wear profile corresponding to the previous "wear geometry step" (the spatial position of each node on both contact surfaces is adjusted in the normal direction by the calculated incremental bilateral wear amounts);
iv. for the i^{th} "wear geometry step", treat the wear loads on the new contact geometry Γ_{c,k^i} for a number of cyles N^i, corresponding to the simulation time $\Delta\tau^i = k^i \times \Delta t$;
v. repeat this procedure incrementally until the desired total number of fretting cycles N_t is reached.

This approach is shown schematically in figure 2. All of these aspects have been integrated *via* a specific *Python* user subroutine coupled to the FE software *Code_Aster* [*].

Remark 1
The present implementation of the wear geometry update is more accurate and efficient than that of [50], [40] and [41]. Whereas the methodology of [41] uses a discrete Lagrange multiplier frictional contact algorithm to strictly enforce the stick-slip conditions, the present one lies on an accurate continuous mixed frictional contact formulation. Wear scars used to update the contact geometry are then expected to be more accurate.

For a flexible finite element analysis of structures submitted to wear that may occur in any place of the structure, it is of primary importance from a cost point of view to be able to change the global numerical model representing a coarse approximation of the whole structure in the vicinity of the worn zone.
The Arlequin method offers high mutiscale modelling potentialities in terms of flexibility and of practical capabilities to locally integrate alterations in global numerical models of engineering

[*]thermo-mechanical FE free software of **Électricité de France**, downloadable at www.code-aster.org

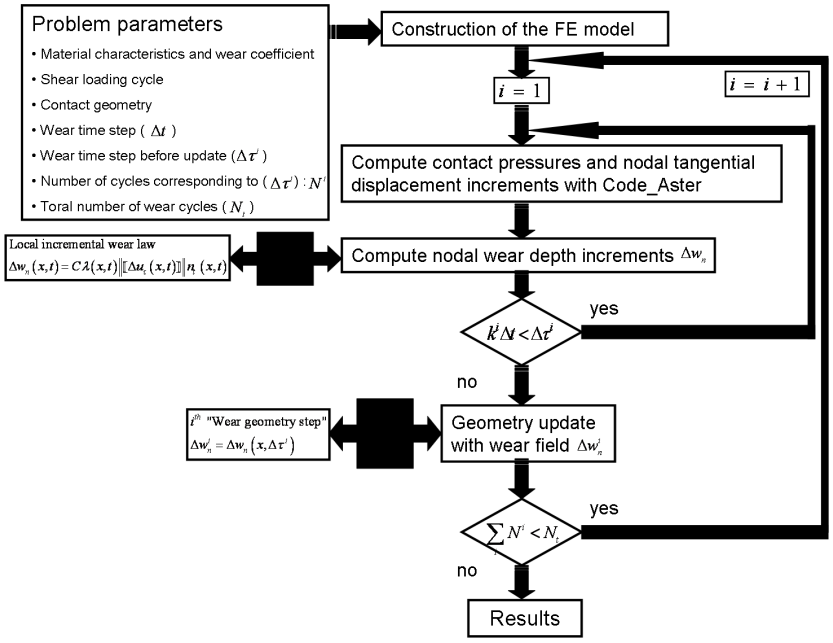

Figure 2. Flow chart of the wear geometry update procedure.

structures.
Application of the Arlequin framework within the suggested incremental wear simulation all with further details on the multiresolution wear strategy constitutes the subject of the following section.

5. THE MULTIMODEL/MULTISCALE STRATEGY

5.1. The Arelquin framework for contact and wear problems

As underlined in [7], [8] and [9], the Arlequin method is a global-local type partition of model framework which allows concurrent multiscale and multimodel analyses.
In the Arlequin framework, a local numerical model is super-imposed to the global one. The former takes into account wear phenomena and is weakly interfaced with the latter. The coexistence of the two different models allows to use :

i. different mesh parameters (multiscale analysis),
ii. different FE models (multimodel analysis),
ii. different mechanical/physical behaviours (multiphysic analysis).

To illustrate this, we consider the linearized elasticity model problem of a solid $\mathcal{B}$, occupying the closure of the domain Ω of $\mathbb{R}^d$, coming into contact with an obstacle O (see figure 3 (a)). The potential contact surface of the solid $\mathcal{B}$ is denoted $\Gamma_{c,t}$.
In order to enlighten a zone of interest $S \subset \Omega$ in the vicinity of the contact surface, we

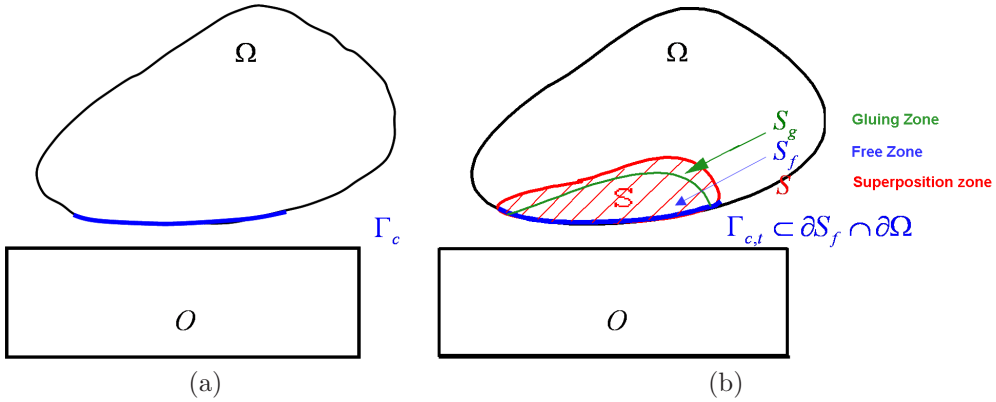

Figure 3. (a) model problem (b) Arlequin coupling.

superpose a local model to the global one in S. The local model or patch is chosen in such a manner that $\Gamma_{c,t} \subset \partial S$ (see figure 3 (b)). To do this, we follow basically the different Arelquin steps :

1. super-impose, in the local zone S, a local model to the global one;
2. let the mechanical energies be splitted in the superposed models, using weight positive parameter functions verifying a partition of unity principle;
3. glue partially, in a subzone S_g of S, the local model to the global one by using a convenient coupling operator;
4. treat the contact in a way compatible with the gluing.

The resulting mixed Arlequin problem to solve reads :
Find $(\boldsymbol{u}^g, \boldsymbol{u}^l, \lambda, \boldsymbol{\Lambda}, \Upsilon; w_n, S_u^w, S_f) \in \mathcal{CA}(\Omega) \times \mathcal{CA}(S) \times H_c \times \boldsymbol{H}_f \times \mathcal{M} \times H_w \times (L^\infty(\Gamma_{c,t}; \{0,1\}))^2 / \forall (\boldsymbol{w}^g, \boldsymbol{w}^l, \lambda^*, \boldsymbol{\Lambda}^*, \Upsilon^*)$

$$\mathbf{G}_{int}(\boldsymbol{u}^g, \boldsymbol{u}^l, \boldsymbol{w}^g, \boldsymbol{w}^l; \alpha) + \mathbf{G}_{cont}(\lambda, \boldsymbol{w}^l) + \mathbf{G}_{fric}(\boldsymbol{\Lambda}, \boldsymbol{w}^l) + \mathbf{G}_{arle}(\Upsilon, \boldsymbol{w}^g, \boldsymbol{w}^l) = \mathbf{G}_{ext}(\boldsymbol{w}^g, \boldsymbol{w}^l; \beta) \tag{47}$$

$$\mathbf{G}_{cont}^{weak}(\boldsymbol{u}^l, \lambda, \lambda^*) = 0 \tag{48}$$

$$\mathbf{G}_{fric}^{weak}(\boldsymbol{u}^l, \boldsymbol{\Lambda}, \boldsymbol{\Lambda}^*) = 0 \tag{49}$$

$$\mathbf{G}_{arle}(\Upsilon^*, \boldsymbol{u}^g, \boldsymbol{u}^l) = 0 \tag{50}$$

with

$$\mathbf{G}_{int}(\boldsymbol{u}^g,\boldsymbol{u}^l,\boldsymbol{w}^g,\boldsymbol{w}^l;\alpha)=\int_\Omega \alpha Tr[\sigma^g(\boldsymbol{u}^g)\epsilon^g(\boldsymbol{w}^g)]d\Omega+\int_S(1-\alpha)Tr[\sigma^l(\boldsymbol{u}^l)\epsilon^l(\boldsymbol{w}^l)]dS \tag{51}$$

$$\mathbf{G}_{cont}(\lambda,w)=-\int_{\Gamma_{c,t}} S_u^w\lambda[\![\boldsymbol{w}_n]\!]d\Gamma \tag{52}$$

$$S_u^w=1_{\mathbb{R}^-}\left(\lambda-\rho_n d_n^{w,l}\right) \tag{53}$$

$$\mathbf{G}_{fric}(\boldsymbol{\Lambda},\boldsymbol{w})=-\int_{\Gamma_{c,t}}\mu S_u^w\lambda\left[S_f\boldsymbol{\Lambda}+(1-S_f)\,\frac{\boldsymbol{\Lambda}+\rho_\tau[\![\boldsymbol{v}_\tau^l]\!]}{\|\boldsymbol{\Lambda}+\rho_\tau[\![\boldsymbol{v}_\tau^l]\!]\|}\right][\![\boldsymbol{w}_\tau]\!]d\Gamma \tag{54}$$

$$S_f=1_{B(0,1)}\big(\boldsymbol{\Lambda}+\rho_\tau[\![\boldsymbol{v}_\tau^l]\!]\big) \tag{55}$$

$$\mathbf{G}_{arle}(\Upsilon^*,\boldsymbol{w}^g,\boldsymbol{w}^l)=(\Upsilon^*,\boldsymbol{w}^g-\boldsymbol{w}^l)_{S_g}\quad((.,.)_{S_g}\ equivalent H^1(S_g)\text{ scalar product}) \tag{56}$$

$$\mathbf{G}_{ext}(\boldsymbol{w}^g,\boldsymbol{w}^l;\beta)=\int_\Omega\beta\boldsymbol{f}.\boldsymbol{w}^g d\Omega+\int_S(1-\beta)\boldsymbol{f}.\boldsymbol{w}^l dS \tag{57}$$

$$\mathbf{G}_{cont}^{weak}(\boldsymbol{u},\lambda,\lambda^*)=-\frac{1}{\rho_n}\int_{\Gamma_{c,t}}\left[\lambda-S_u^w\left(\lambda-\rho_n d_n^{w,l}\right)\right]\lambda^* d\Gamma \tag{58}$$

$$\begin{aligned}\mathbf{G}_{fric}^{weak}(\boldsymbol{u},\boldsymbol{\Lambda},\boldsymbol{\Lambda}^*)=\frac{1}{\rho_\tau}\int_{\Gamma_{c,t}}\mu S_u^w\lambda\Big[\boldsymbol{\Lambda}-[S_f\left(\boldsymbol{\Lambda}+\rho_\tau[\![\boldsymbol{v}_\tau^l]\!]\right)+(1-S_f)\,\frac{\boldsymbol{\Lambda}+\rho_\tau[\![\boldsymbol{v}_\tau^l]\!]}{\|\boldsymbol{\Lambda}+\rho_\tau[\![\boldsymbol{v}_\tau^l]\!]\|}]\Big]\boldsymbol{\Lambda}^*d\Gamma\\ +\int_{\Gamma_{c,t}}(1-S_u^w)\,\boldsymbol{\Lambda}\boldsymbol{\Lambda}^*d\Gamma=0\end{aligned} \tag{59}$$

where the g and l superscripts refer to the global and local quantities, respectively and where α et β are energy weight parameter functions verifying the following properties :

$$\alpha=\beta=1\quad\text{in}\quad\Omega\setminus S \tag{60}$$

$$0\le\alpha,\beta\le 1\quad\text{in}\quad S \tag{61}$$

In the new (bi)model simulation, the contact and wear phenomena are totally attributed to the local model which is coupled to the global one by means of the energy coupling operator $\mathbf{G}_{arl}$.

The functional space $\mathcal{M}$ is defined by :

$$\mathcal{M}=(H^1(S_g))^2$$

This definition corresponds to a treatment of the Arlequin constraints by H^1 Lagrange multipliers (see [9] and [**?**] for further insights and theoretical details related to this important coupling aspect).

When using the Arlequin method, the local model (which encompasses the frictional wear contact phenomena) is put forward by choosing α "nearly" equal to zero in the free zone S_f. The two models "living" in the superposition zone can be approximated quite differently. This implies that one can keep a global "coarse" numerical approximation of an engineering product while introducing with great flexibility the refinements required by the analyses of localized

phenomena.
The relevance of the Arlequin approach in dealing with contact problems involving wear is exemplified in this section through three important issues, namely :

1. the delocalization of the wear law to address the singularity of wear profiles and their mesh-dependency near the contact edges;
2. the local unilateral/bilateral geometry update (without any change of the global sound mesh) to account for material removal due to wear;
3. the multimodel analysis of contacting thin structures submitted to wear phenomena that may occur in any place of the structure.

5.2. Nonlocality of Archard's model at the contact edges

It is well known that, due to the use of local Archard's model, the numerical wear fields which can be calculated by discretizing it by means of the classical FEM show mesh-dependency near the contact edges. To address the singularity of wear profiles, the wear law is here delocalized close to the contact edges.
For the sake of efficiency, it is of primary importance to be able to achieve the zoom operation (inducing mesh-dependency) without remeshing the underlying global numerical model. Then the delocalizing wear law is introduced in the neighborhood of the local zone by means of a narrowly refined Arlequin patch.

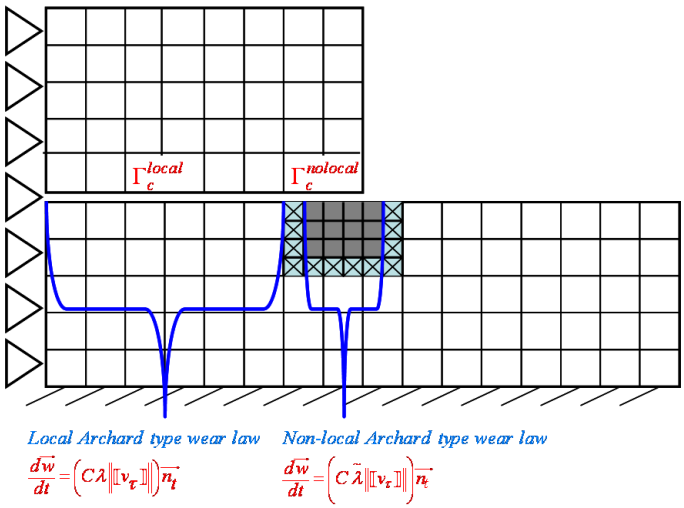

Figure 4. Nonlocality of Archard's type wear law in the Arlequin framework.

As represented in figure 4, the proposed methodology consists in :

- splitting the contact zone $\Gamma_{c,t}$ into two parts denoted $\Gamma_{c,t}^{local}$ and $\Gamma_{c,t}^{nonlocal}$ and verifying :
  - $\overline{\Gamma}_{c,t}^{local} \cup \overline{\Gamma}_{c,t}^{nonlocal} = \overline{\Gamma}_{c,t}$;
  - $\Gamma_{c,t}^{local} \bigcap \Gamma_{c,t}^{nonlocal} = \emptyset$.

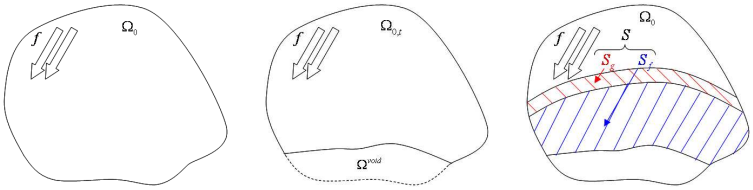

Figure 5. (a) Unworn solid (b) Worn solid (c) Arlequin model superposition.

- using local Archard's model for $\Gamma_{c,t}^{local}$ (corresponding to the coarse underlying mesh away from the contact edges), ie. :

$$\frac{dw_n(\boldsymbol{p},t)}{dt} = C\lambda \left\| [\![\boldsymbol{v}_\tau]\!] \right\| \text{ for } \boldsymbol{p} \in \Gamma_{c,t}^{local} \tag{62}$$

- using an "averaged" nonlocal wear law of Archard's type for $\Gamma_{c,t}^{nonlocal}$ (corresponding to the narrowly refined Arlequin patch in the vicinity of contact edges), ie. :

$$\frac{dw_n(\boldsymbol{p},t)}{dt} = C\widetilde{\lambda} \left\| [\![\boldsymbol{v}_\tau]\!] \right\| \text{ for } \boldsymbol{p} \in \Gamma_{c,t}^{nonlocal} \tag{63}$$

In (63), $\widetilde{\lambda}$ is a contact pressure distribution resulting from a rather classical averaging technique of the local pressure distribution λ in a fixed local zone whose length is l near contact edges. For a 2D case, and for all $x \in \Gamma_{c,t}^{nonlocal}$, the "averaging" procedure is achieved in the zone $B(x,\delta) \cap \Gamma_{c,t}$ where $B(x,\delta)$ is the ball whose center is x and radius is δ. The δ parameter should be calibrated to meet experimentally measured wear profiles. The principle that lies behind this phenomenological remedy is the following : when a specific point (the contact edge in this case) displays high wear evolution, we decide to slow down this wear evolution so that it drops to a mean evolution equivalent to that of neighboring contact points.
A numerical test is given in subsection 6-2 to exemplify this wear delocalizing procedure.

5.3. Wear material removal in the Arlequin framework

When the material removal from solid surfaces due to wear actions is relatively small, the only correction of the contact gap field might be sufficient to simulate the wear evolution front. Nevertheless, when the wear amounts are not negligible, this primary analysis may suffer precision. A remeshing (eventually adaptive meshing) framework is often used to account for physical material loss. For a flexible simulation of the surface wear evolution, we use the Arlequin approach.

To illustrate this, let's consider the sound solid represented by figure 5 (a). The formulation of this model problem reads :

$$\begin{aligned} &\text{Find} \quad \boldsymbol{u} \in \mathcal{CA}(\Omega_0) \quad \text{such that for all} \quad \boldsymbol{w} \in \mathcal{CA}(\Omega_0) \\ &\mathbf{G}_{int}(\boldsymbol{u},\boldsymbol{w}) = \mathbf{G}_{ext}(\boldsymbol{w}) \end{aligned} \tag{64}$$

where $\mathcal{CA}(\Omega_0)$ is the space of kinematically admissible displacements and where $\mathbf{G}_{int}$ and $\mathbf{G}_{ext}$ are the virtual works of internal and external forces, respectively.

Let's suppose that the solid $\mathcal{B}$ experiences the removal of a part $\mathcal{B}^{void}$ of its material, occupying the closure of a sub-domain Ω^{void} (figure 5 (b)). The worn solid occupies the closure of the domain $\Omega_{0,t}$ of $\mathbb{R}^2$. In order to model $\Omega_{0,t}$, we super-impose to the sound model Ω_0 a local model $\mathcal{L}$ which geometry reflects the material loss (cf. figure 5 (c)). Then, following the different steps of the Arlequin approach, we :

- duplicate the mechanical fields in S,
- let the mechanical energies be shared in S by the superposed models.
- couple the two states in a sub-zone S_g of S (figure 5 (c)).

Since the superposition zone S is chosen in such a manner that it lies in the sound solid $\mathcal{B}$, then the weight affected to Ω^{void} will be $\alpha \approx 0$ and the internal work $\int_{\Omega^{void}} \alpha Tr[\sigma^g(\boldsymbol{u}^g)\epsilon^g(\boldsymbol{w}^g)]d\Omega$ corresponding to the lost material is almost zero.

While keeping a global FE model with the unchanged initial geometry (and, consequently, a fixed global coarse mesh), insert a local geometrically-adapted Arlequin patch, i.e. a local model whose geometry is updated according to the wear scar. Whereas the methodology of [40] uses a single global mechanical field-based formulation and Multi-Point constraints to glue the super-imposed "wear patch", the present methodology uses one local and one global coupled mechanical fields and ad-hoc coupling operators in the Arlequin framework.

An illustration of the Arlequin-based wear geometry update procedure is given in subsection 6-2.

5.4. Wear of thin structures

Thin structures subjected to wear may experience contact loads that are so localized that their analysis by means of a thin structure FE model would be irrelevant. In the Arlequin framework, one can use a fine 3D FE approximation with a fretting wear law for the local model while keeping a coarse plate-based FE approximation for the global model. For purpose of clear illustration, let's consider a plate clamped at its ends and occupying the closure of the domain $\mathcal{S} = \omega_{plq} \times]-\frac{e}{2}, \frac{e}{2}[$ (see figure 6). The formulation of the fretting wear problem of a

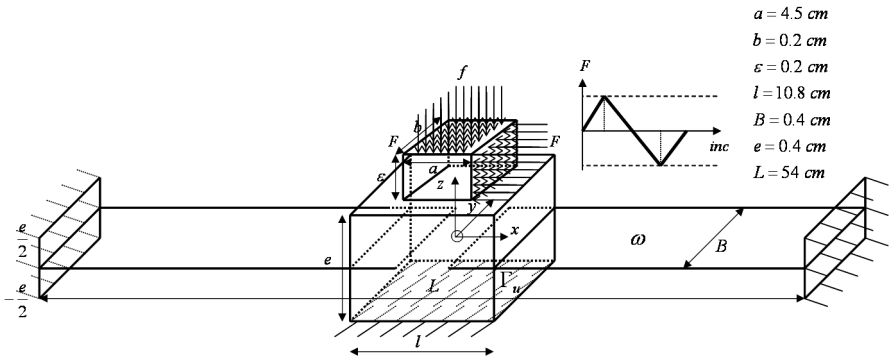

Figure 6. Fretting wear with a mixed plate/3D Arlequin (bi)model.

mixed Arlequin 3d/plate (bi)model by a rigid indenter reads :

Find $\left(\boldsymbol{u}^{\Omega}, \boldsymbol{u}^{\mathcal{S}}, \lambda, \boldsymbol{\Lambda}, \Upsilon; w_n, S_u^w, S_f\right) \in \boldsymbol{CA}(\Omega) \times \boldsymbol{CA}(\mathcal{S}) \times H_c \times \boldsymbol{H}_f \times \boldsymbol{M} \times H_w \times \left(L^{\infty}(\Gamma_{c,t}; \{0,1\})\right)^2 / \forall \left(\boldsymbol{w}^{\Omega}, \boldsymbol{w}^{\mathcal{S}}, \lambda^*, \boldsymbol{\Lambda}^*, \Upsilon^*\right) \in \boldsymbol{CA}(\Omega) \times \boldsymbol{CA}(\mathcal{S}) \times H_c \times \boldsymbol{H}_f \times \boldsymbol{M}$;

$$\begin{aligned} &\boldsymbol{G}_{int}\left(\boldsymbol{u}^{\Omega}, \boldsymbol{w}^{\Omega}, \boldsymbol{u}^{\mathcal{S}}, \boldsymbol{w}^{\mathcal{S}}, \alpha\right) + \boldsymbol{G}_{cont}\left(\lambda, \boldsymbol{w}^{\mathcal{S}}\right) + \boldsymbol{G}_{fric}\left(\boldsymbol{\Lambda}, \boldsymbol{w}^{\mathcal{S}}\right) + \boldsymbol{G}_{arle}\left(\Upsilon, \boldsymbol{w}^{\Omega}, \boldsymbol{w}^{\mathcal{S}}\right) = \\ &\qquad\qquad \boldsymbol{G}_{ext}\left(\boldsymbol{w}^{\Omega}, \boldsymbol{w}^{\mathcal{S}}, \beta\right) \end{aligned} \tag{65}$$

$$\boldsymbol{G}_{arle}\left(\Upsilon^*, \boldsymbol{u}^{\Omega}, \boldsymbol{u}^{\mathcal{S}}\right) = 0 \tag{66}$$

$$\boldsymbol{G}_{cont}^{weak}\left(\lambda, \lambda^*, \boldsymbol{u}^{\mathcal{S}}\right) = 0 \tag{67}$$

$$\boldsymbol{G}_{fric}^{weak}\left(\boldsymbol{\Lambda}, \boldsymbol{\Lambda}^*, \boldsymbol{u}^{\mathcal{S}}\right) = 0 \tag{68}$$

with :

$$\boldsymbol{G}_{int}\left(\boldsymbol{u}^{\Omega}, \boldsymbol{w}^{\Omega}, \boldsymbol{u}^{\mathcal{S}}, \boldsymbol{w}^{\mathcal{S}}, \alpha\right) = \int_{\Omega} (1-\alpha)\sigma_{\alpha\beta}^{\Omega}\partial_{\beta}\boldsymbol{w}_{\alpha}^{\Omega} d\Omega + \int_{\mathcal{S}} \alpha\sigma_{ij}^{\mathcal{S}}\partial_j \boldsymbol{w}_i^{\mathcal{S}} d\mathcal{S} \tag{69}$$

$$\boldsymbol{G}_{ext}\left(\boldsymbol{w}^{\Omega}, \boldsymbol{w}^{\mathcal{S}}, \beta\right) = \int_{\Omega} (1-\beta)\boldsymbol{f}^{\Omega}\boldsymbol{w}^{\Omega} d\Omega + \int_{\mathcal{S}} \beta \boldsymbol{f}^{\mathcal{S}}\boldsymbol{w}^{\mathcal{S}} d\mathcal{S} \tag{70}$$

$$\boldsymbol{G}_{arle}\left(\Upsilon^*, \boldsymbol{w}^{\Omega}, \boldsymbol{w}^{\mathcal{S}}\right) = \langle \Upsilon^*, \boldsymbol{w}^{\mathcal{S}} - \boldsymbol{w}^{\Omega}\rangle_{S_g} \tag{71}$$

$$\boldsymbol{G}_{cont}\left(\lambda, \boldsymbol{w}^{\mathcal{S}}\right) = -\int_{\Gamma_{c,t}} S_u^w \lambda [\![\boldsymbol{w}_n^{\mathcal{S}}]\!] d\Gamma \tag{72}$$

$$\boldsymbol{G}_{fric}\left(\Lambda, \boldsymbol{w}^{\mathcal{S}}\right) = -\int_{\Gamma_{c,t}} \mu S_u^w \lambda \left[S_f \Lambda + (1-S_f)\frac{\Lambda + \rho_\tau [\![\boldsymbol{v}_\tau^{\mathcal{S}}]\!]}{\|\Lambda + \rho_\tau [\![\boldsymbol{v}_\tau^{\mathcal{S}}]\!]\|}\right] [\![\boldsymbol{w}_\tau]\!] d\Gamma \tag{73}$$

$$\boldsymbol{G}_{cont}^{weak}\left(\lambda, \lambda^*, \boldsymbol{u}^{\mathcal{S}}\right) = -\frac{1}{\rho_n}\int_{\Gamma_{c,t}} \left\{\lambda - S_u^w\left(\lambda - \rho_n d_n^{w,\mathcal{S}}\right)\right\} \lambda^* d\Gamma \tag{74}$$

$$\tag{75}$$

$$\begin{aligned} \boldsymbol{G}_{fric}^{weak}\left(\Lambda, \Lambda^*, \boldsymbol{u}^{\mathcal{S}}\right) = \frac{1}{\rho_\tau}\int_{\Gamma_{c,t}} \mu S_u^w \lambda \Bigg[\Lambda - [S_f\left(\Lambda + \rho_\tau [\![\boldsymbol{v}_\tau^{\mathcal{S}}]\!]\right) + (1-S_f)\frac{\Lambda + \rho_\tau [\![\boldsymbol{v}_\tau^{\mathcal{S}}]\!]}{\|\Lambda + \rho_\tau [\![\boldsymbol{v}_\tau^{\mathcal{S}}]\!]\|}]\Bigg] \Lambda^* d\Gamma \\ + \int_{\Gamma_{c,t}} (1 - S_u^w)\Lambda\Lambda^* d\Gamma = 0 \end{aligned} \tag{76}$$

and where :

$$S_u^w = 1_{\mathbb{R}^-}\left(\lambda - \rho_n d_n^{w,\mathcal{S}}\right) \tag{77}$$

$$S_f = 1_{B(0,1)}\left(\mathbf{\Lambda} + \rho_\tau [\![\boldsymbol{v}_\tau^{\mathcal{S}}]\!]\right) \tag{78}$$

$$\sigma_{ij}^{\mathcal{S}} = \frac{E}{1+\nu}\left\{\gamma_{ij}\left(\boldsymbol{u}^{\mathcal{S}}\right) + \frac{\nu}{1-2\nu}\gamma_{kk}\left(\boldsymbol{u}^{\mathcal{S}}\right)\delta_{ij}\right\}(1 \leq i,j \leq 3) \tag{79}$$

$$\sigma_{\alpha\beta}^{\Omega} = \frac{E}{1+\nu}\left\{\gamma_{\alpha\beta}\left(\boldsymbol{u}^{\Omega}\right) + \frac{\nu}{1-\nu}\gamma_{\mu\mu}\left(\boldsymbol{u}^{\Omega}\right)\delta_{\alpha\beta}\right\}(1 \leq \alpha,\beta \leq 2) \tag{80}$$

$$\sigma_{\lambda 3}^{\Omega} = \sigma_{3\lambda}^{\Omega} = \frac{\kappa E}{1+\nu}\gamma_{\lambda 3}\left(\boldsymbol{u}^{\mathbf{\Omega}}\right) \ (\kappa \text{ being a correction factor and } 1 \leq \lambda \leq 2) \tag{81}$$

$$\boldsymbol{CA}\left(\mathcal{S}\right) = \left\{\boldsymbol{v}^{\mathcal{S}} \in H^1(\mathcal{S});\ \boldsymbol{v}_{|\Gamma_u}^{\mathcal{S}} = 0\right\} \tag{82}$$

$$\boldsymbol{CA}\left(\Omega\right) = \left\{\boldsymbol{v} = \boldsymbol{v}^0 + z\boldsymbol{v}^1; \boldsymbol{v}^0 \in \left(H^1(\omega)\right)^3; \boldsymbol{v}^1 \in \left(H^1(\omega)\right)^2, |z| < \frac{e}{2}; \left| \begin{array}{l} \boldsymbol{v}^0(\{0;L\},y) = 0 \\ \boldsymbol{v}^1(\{0;L\},y) = 0 \end{array} \right. \right\} \tag{83}$$

$$\boldsymbol{M} = \boldsymbol{CA}\left(\Omega\right)_{|S} \tag{84}$$

The space of gluing forces is taken as the restriction to the gluing zone of the space of admissible plate fields.

To show the potential of our multiresolution strategy, some numerical experimentations are carried out and results are shown in the next section.

6. NUMERICAL RESULTS

A two-dimensional elastic block problem is chosen to demonstrate the feasibility and the relavance of the multiscale/multimodel finite element analysis of the two-dimensional fretting wear problem. The numerical example, depicted in figure 7 and already treated in [24, 36], consists in wearing contact interaction of a $5 \times 0.5\ cm^2$ elastic block. The block is fixed at the left end and unilaterally constrained by a rigid support at the bottom. It is also subjected to the surface loads f and F. f is a given normal pressure acting at the top of the block and F is a shearing cyclic load acting on the right edge of the block, with an amplitude of 10 daN/mm according to the right part of figure 7. This type of boundary conditions in wear problems is called fretting condition. The block and the support are approximated by 16×10 and 32×10 four-nodes bilinear finite elements, respectively. The potential contact surface at the bottom of the block is approximated by 16 1D linear finite elements using the trapezoidal quadrature rule in such a manner that the integration points coincide with the nodal displacement points of the contact surface. This particular choice of the nodes located on the boundary Γ_{ch} allows the recovering of the well-known node-on-facet strategy. Each shear cycle is discretized by $n_{incr} = 4$ "time steps" or increments. Classical linearized elasticity is assumed. We have taken a Young's modulus, a Poisson ratio and friction and wear coefficients equal to 210 GPa, 0.3, 0.3 and $1.0 \times 10^{-11}\ Pa^{-1}$, respectively.
In the sequel, several variants of this numerical test are achieved :

i. The first stresses the mesh-dependency of the wear profile induced by the locality of

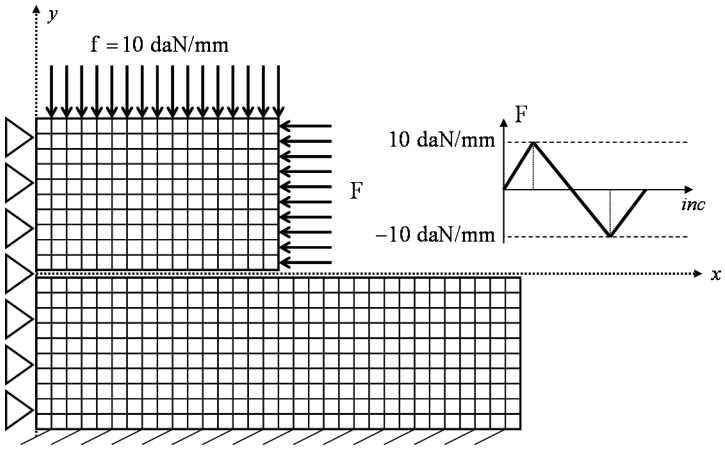

Figure 7. A 2D elastic block subjected to given normal and shear cyclic loads.

Archard's model in the vicinity of the contact edge and assesses the effectiveness of the wear delocalization in the Arlequin framework.

ii. The point of focus of the second is the illustration, in the Arlequin framework, of the (unilateral) wear geometry update of the "slave" contacting surface by means of a geometrically-adapted local patch reproducing the worn interface.

iii. The third explores the differences between unilateral and bilateral wear, combined with the wear-related geometry update.

iv. The fourth considers the fretting wear for a mixed 3d/plate (bi)model.

6.1. Nonlocality of Archard's model

The academic fretting test depicted in figure 7 is used here to show the potential of the wear delocalizing strategy. The contact surface $\Gamma_{c,t}$ corresponds to $x \in [0, 5]$ cm. Since a steep stress distribution gradient was expected around the contact edge, the size of the FE mesh thereby was dealt with separately from the global contact region. Two different meshes are considered :

- a coarse mesh (32×10 QUAD4 bilinear finite elements for the upper solid and 64×10 bilinear finite elements for the support),
- a fine Arlequin patch towards the contact edge (the refinement is done over the distance $[3.6875, 5.3125]$ cm and the resulting mesh contains 32×10 bilinear finite elements for the upper block and 64×10 and 24×6 bilinear finite elements for the support).

Local and delocalized Archard's type wear laws are used for both models. The length of the nonlocal wear zone is $l = 1$ cm (i.e. $\Gamma_{c,t}^{local} = [0, 4]$ cm and $\Gamma_{c,t}^{nonlocal} = [4, 5]$ cm). The parameter δ is equal to 0.3125 cm. For this particular choice, the averaging is achieved in a crown of two elements around each point of $\Gamma_{c,t}^{nonlocal}$.

The results plotted in figure 8 show that the solution of local Archard's law "explodes" with the refinement level while the one corresponding to nonlocal Archard's type law seems to

stabilize.

In order to confirm the effectiveness of the suggested wear delocalizing methodology, the

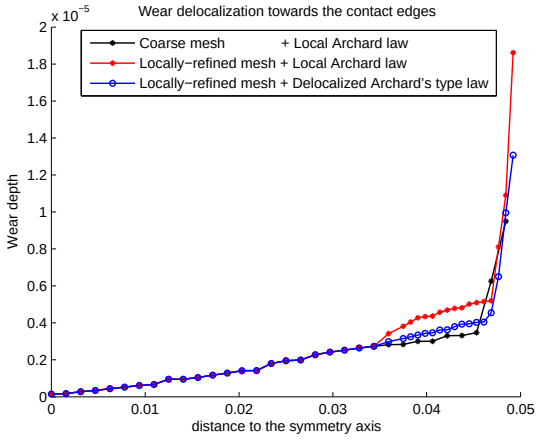

Figure 8. Nonlocality of Archard's wear law.

wear profiles must converge with respect to the local mesh size. Four different locally-refined FE models corresponding to 4 different mesh parameters are used, while conserving the same nonlocal length zone $l = [4, 5]$ cm and the same averaging radius $\delta = 0.3125$ cm.

Figure 9 depicts the wear scars corresponding to the 4 FE models encompassing either of the wear laws. We notice that the wear profiles corresponding to local Archard's model are mesh-dependent whereas those corresponding to the nonlocal wear law are nolonger mesh-dependent and stabilize (helpfully) despite the narrower refinement in the neighborhood of the contact edges. Owing to the wear delocalizing methodology, the concentration of wear depths near to the contact edges (due to the use of local Archard's model within a linearized elasticity framework) is alleviated, thus recovering more physically realistic stresses. Consequently, more stabilized wear front progression is expected. This result confirms the hypothesis put forward by various authors [51] that a mean contact pressure distribution can be convenient to recover a homogenous evolution of the wear damage.

6.2. Application of the Arlequin framework to the wear material removal

In this section, we exemplify the feasibility and the relevance of the wear geometry update in the Arlequin framework. Here, the wear-related geometry update procedure is unilaterally applied to the "slave" block contacting surface of the numerical test represented by figure 7. For this test, the developed finite element method has been applied up to $N_t = 100$ fretting cycles with an acceleration factor $\Delta N^i = \Delta N = 10$. Each "representative" fretting cycle is discretized into $n^i_{incr} = n_{incr} = 4$ increments.

Resulting wear depth and normal contact pressure distributions with and without unilateral wear-related geometry update are plotted in figure 10. It is worth mentioning that the Arlequin-based contact geometry update leads to sharper stress gradients and deeper wear depths at

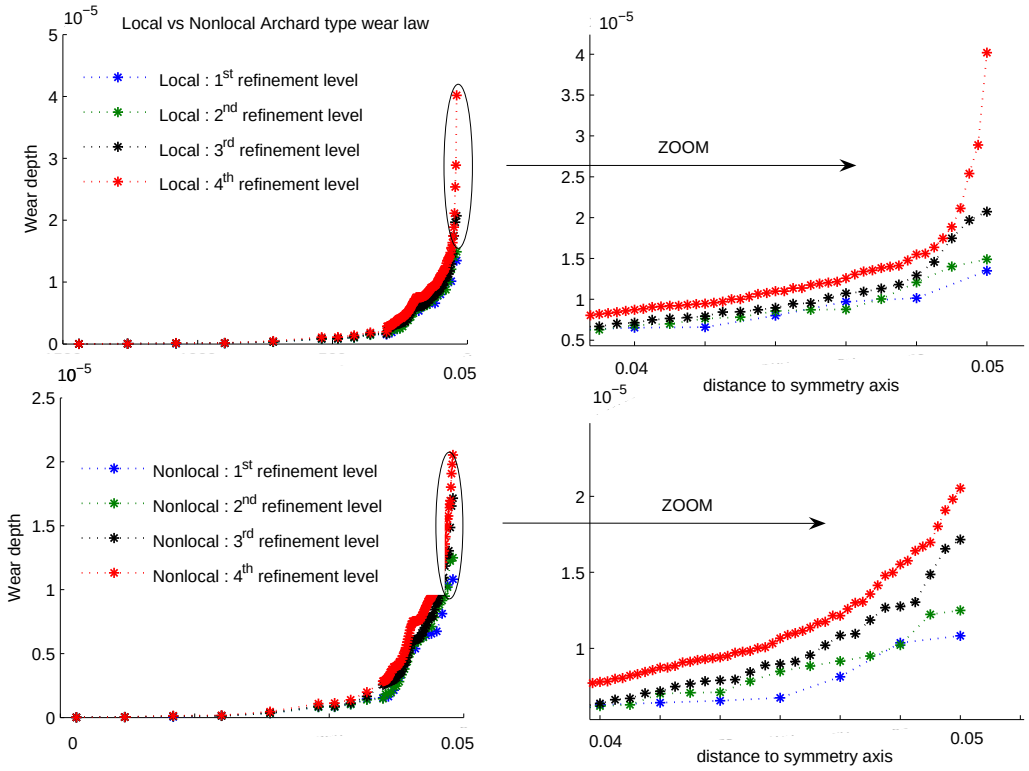

Figure 9. Stabilized wear scars with the mesh for the delocalized wear law.

the leading contact edge. The stress singularity seems to sharpen at the physical boundaries when the effective worn contact geometries are taken into account. This can be explained by the material removal. The fretting wear loading conditions being unchanged, the "burden" that was supported by the lost material is attributed to the remaining material.
Amongst other reasons explaining the local sharp stress variations mentioned above, one can point out the fact that the rigid support is not wearing out and that its geometry is not updated. In the next subsection, we consider bilateral wear and bilateral related geometry update.

6.3. Unilateral vs bilateral wear and geometry update

We consider the same model problem of figure 7 and we assume that the support is wearing out even if the amount of material lost form the rigid support is relatively small when compared to the elastic block. The wear coefficients used in Archard's wear laws are $C^1 = 1.0 \times 10^{-11}\ Pa^{-1}$ and $C^2 = 1.0 \times 10^{-12}\ Pa^{-1}$. 2D wear computations that are identical with one exception are compared. In the first one, wear is calculated only on the slave elastic block (unilateral wear) whereas, in the second one, wear is calculated on both slave elastic block and master rigid support (bilateral wear). Results in figure 11 (b) show that, under bilateral wear assumption,

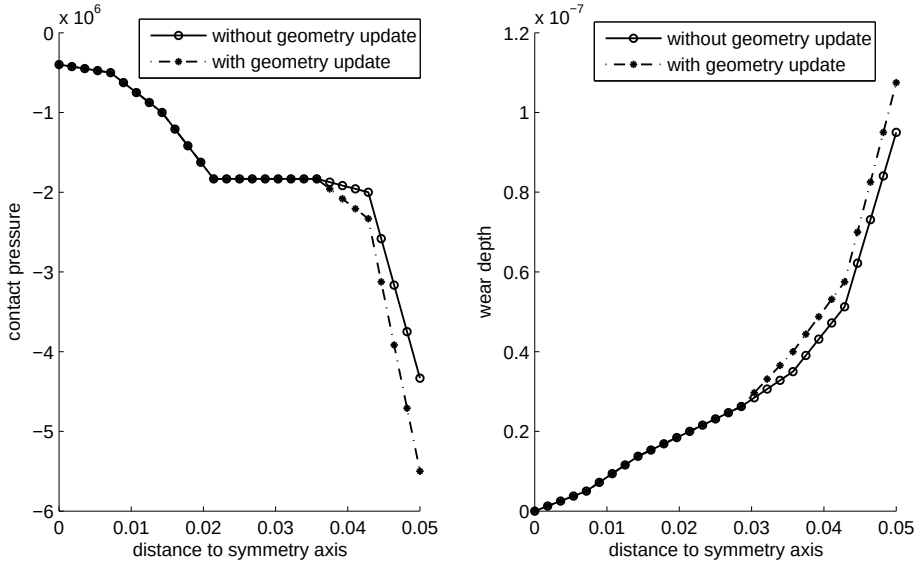

Figure 10. Wear depth and normal contact pressure distributions with and without unilateral wear-related geometry update.

the rigid support is actually worn out. As for the elastic block, wear patterns are donut-shaped with large values at the contact edges. Contact pressures corresponding to unilateral

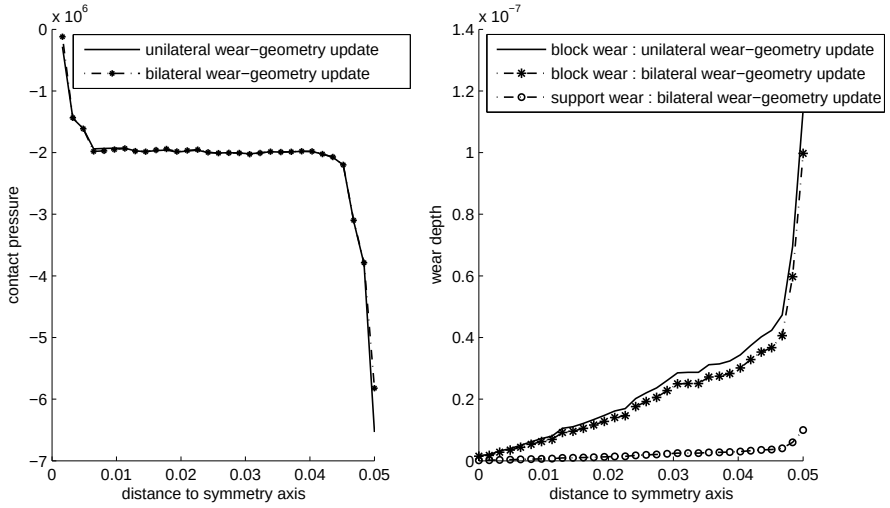

Figure 11. Tool wear hypothesis and geometry update : (a) Contact pressure distribution of the elastic block (b) Wear depth profiles of the elastic block and the rigid support.

and bilateral wear are depicted in figure 11 (a). At the leading contact edge, one can notice that bilateral wear hypothesis gives rise to contact stress gradients that are weaker than unilateral wear does. The appreciable flattening effect observed on the wear profiles can be directly related to the rounded edges of the local geometrically-adapted patchs and to the inherent increase of the surface conformity yielding to the wear processes.

6.4. Wear of thin structures

The Arlequin framework is used in the following example to exemplify the coupling potentiality of a 3D model to a plate one in the vicinity of the wearing contact zone. The mechanical test depicted in figure 6 consists in considering independent global plate and local 3D FE models for the clamped wearing out structure, and in superimposing them through the Arlequin framework. The meshes of the superimposed models are independent. The mean surface ω_{plq} of the global plate model is meshed using 50 QUAD4 bilinear elements. The Arlequin 3D patch and the rigid indenter are meshed with $18 \times 7 \times 8$ and $12 \times 4 \times 4$ eight-node quadrilateral brick elements, respectively.
Figure 12 depicts the restriction of the wear profiles to the (free part of the) superposition zone of the mixed plate/3D (bi)model. It is worth noticing that the $(x, 0, z)$ plane corresponds

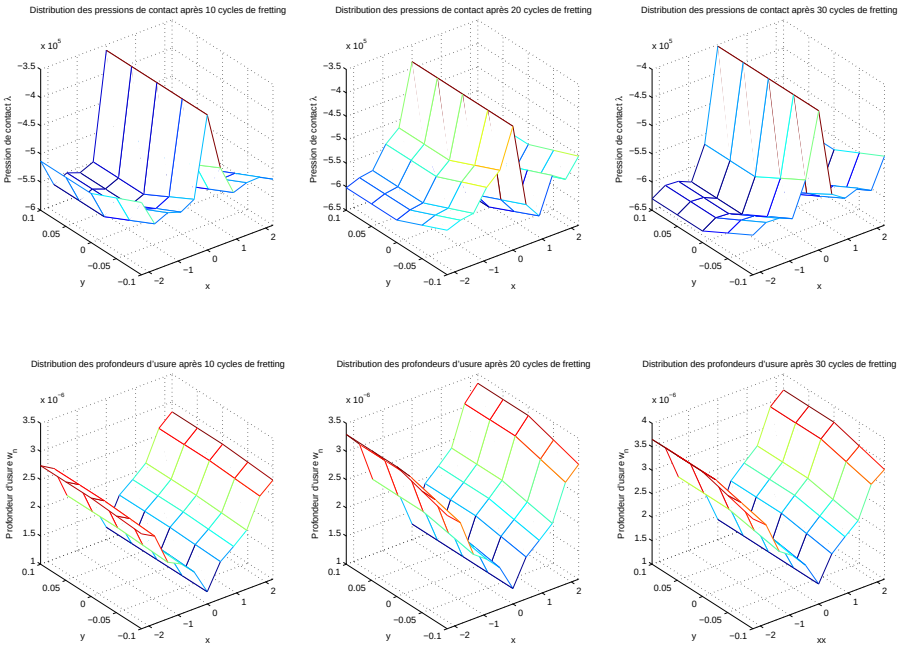

Figure 12. Contact pressure and wear depth distributions on the contacting surface after 10, 20 and 30 fretting cycles.

to the one where the localization is the most critical.
Figure 13 represents the restriction to the $(x, 0, z)$ plane of the wear profiles obtained with an equivalent complete 3D (mono)model and the mixed Arlequin (bi)model. Here, for instance,

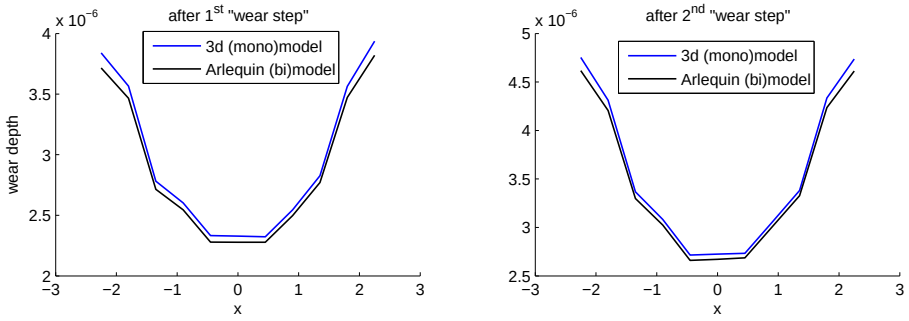

Figure 13. Comparison of wear depth patterns between the fine 3D (mono)model and the Arlequin mixed plate/3D (bi)model.

it is important to underline similarity between the two obtained wear patterns.
Moreover, figure 14 shows that the resulting mixed plate/3D Arlequin (bi)model can display significant through-the-thickness stresses.

7. CONCLUDING REMARKS

In this paper, classical Archard's model is shown to be nonlocal in the vicinity of the contact edges. Delocalized Archard's type wear law leads to more realistic wear profiles. In addition, some multimodel/multiscale numerical wear simulations have been explored in the Arlequin framework :

- Fretting simulations taking into account the contact geometry change due to material removal by wear *via* geometrically-adapted Arlequin patchs have been performed.
- The recalled wear simulation tool, well-established for 2D/3D solids, is extended in the Arlequin framework to analyze fretting wear phenomena of thin structures.

This implies that one can potentially keep a global numerical thin structure-based approximation of a global wearing out engineering product far from the critical contact zones while introducing and piloting, dynamically and with great flexibility, the multiscale/multimodel refinements required by the localized contact phenomena involving wear.

The repeating sharp stresses in oscillatory sliding contact can give rise to localized contact plastic deformations and local fatigue failure. Linearized elasticity assumed in our primary analysis is not sufficiently relevant to provide a precise description of these severe local weakness mechanisms that might cause crack initiation and nucleation (see e.g. [20, 21]). These limiting assumptions suggest that future works need to focus on a better intergration of more enriched physical behaviours to provide a more pertinent prediction of wear depth and damage evolution.

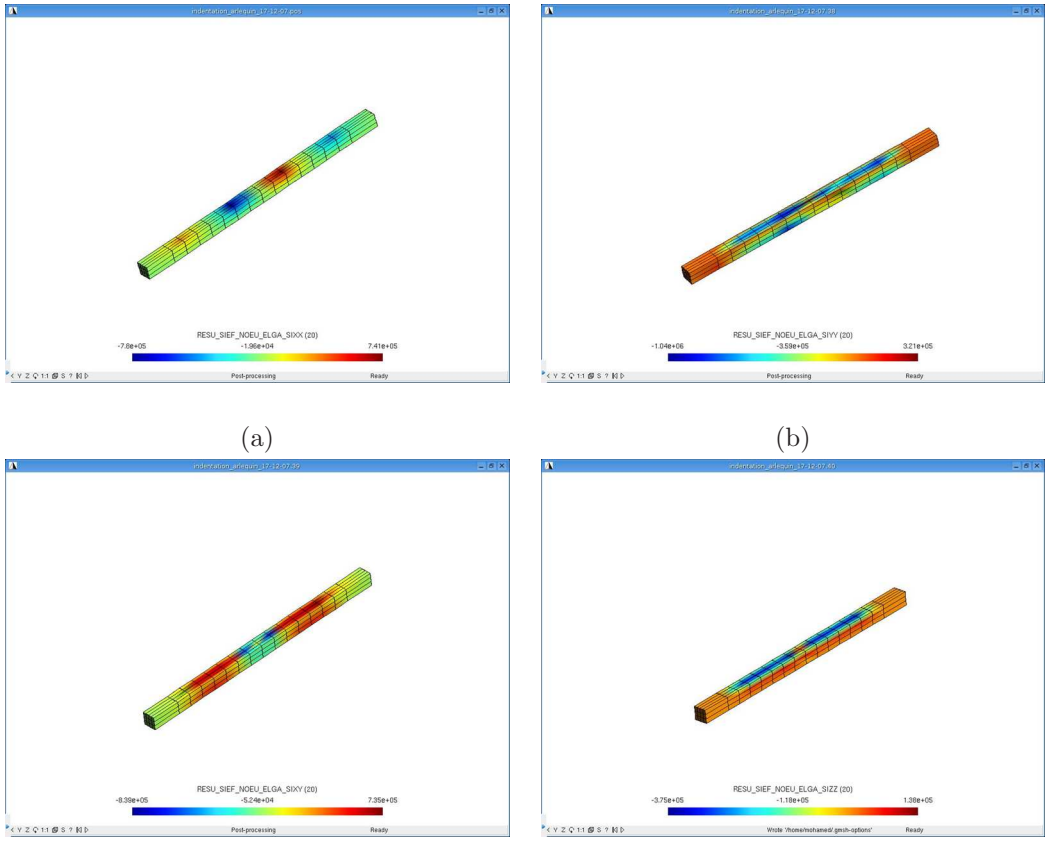

Figure 14. (a) σ_{xx} (b) σ_{yy} (c) σ_{xy} (d) σ_{zz}.

ACKNOWLEDGEMENTS

The support of Électricité de France is gratefully acknowledged.

REFERENCES

1. Simo JC, Laursen TA. An augmented Lagrangian treatment of contact problems involving friction, *Computer and Structures* 1992; **42**:97–116.
2. Klarbring A. Large displacement frictional contact: a continuum framework for finite element discretization, *European Journal of Mechanics A/solids* 1995; **2**:237–253.
3. Curnier A, He Q.-Ch, Klarbring A. Continuum mechanics modelling of large deformation contact wit friction, in *Contact Mechanics* 1995; **7**:145–158.
4. Wriggers P. *Computational Contact Mechanics*, J. Wiley & Sons, New York, 2002.
5. Laursen TA. *Computational Contact and Impact Mechanics: Fundamentals of Modeling Interfacial Phenomena in Nonlinear Finite Element Analysis*, Springer-Verlag, Heidelberg, 2002.

6. Ben Dhia H, Zarroug M. Hybrid frictional contact particles-in elements, *Revue Européenne des éléments finis* 2002; **9**:417–430.
7. Ben Dhia H. Multiscale mechanical problems : the Arlequin method, *Comptes rendus de l'académie des sciences série IIb* 1998; **326**:899–904.
8. Ben Dhia H. Numerical modeling of multiscale mechanical problems : The Arlequin method. *ECCM Mnchen* 1999.
9. Ben Dhia H, Rateau G. The Arlequin method as a flexible engineering design tool, *International Journal for Numerical Methods in Engineering* 2005; **62**:1442–1462.
10. Ben Dhia H. and Zammali C. *Level-Set*s fields, placement and velocity-based formulation of contact-impact problems. *International Journal for Numerical Methods in Engineering* 2007; **69**:2711–2735.
11. Gassner E. The value of surface-protective media againt fretting corrosion on the basis of fatigue strength tests. *Laboratorium for Betriebsfestigkeit TM19/67* 1967.
12. Buch A. Fatigue and fretting of pin-lug joints with and without interference fit. *Wear* 1977: 43–49.
13. Hattori T., Kawai S., Okamoto N., Sonobe T. Torsional fatigue strength of a shrink-fitted shaft. *Bull JSME* 1981;24(197):1893.
14. Johnson R. L., Bill R. C. Fretting in aircraft turbine engines. *NASA TM X-71606* 1974.
15. Hattori T., Sakata S., Ohnishi H. Slipping behaviour and fretting fatigue in the disk/blade dovetail region. *Proc. of the 1983 Tokyo international gas turbine congress* 1984: 945.
16. Archard J. F. Contact and rubbing of flat surfaces. *J. Appl.Phys* 1953; **24**:981–988.
17. Araujo J. A., Nowell D. The effect of rapidly varying contact stress fields on fretting fatigue. *Int. J. Fatigue* 2002 **24**:763–775.
18. Fellows L. J., Nowell D., Hills D. A. On the initiation of fretting fatigue cracks. *Wear* 1997 **205**:120–129.
19. Hattori T., Nakamura M. Fretting-fatigue evaluation using stress-singularity parameters at contact edges. *Tribology International* 1994; **18**:453.
20. Hattori T., Nakamura M., Watanabe T. Simulation of fretting-fatigue life by using stress-singularity parameters and fracture mechanics. *Tribology International* 2003; **36**:87–97.
21. Hattori T., Watanabe T. Fretting fatigue strength estimation considering the fretting wear process. *Tribology International* 2006; **39**:1100–1105.
22. Agelet de Saracibar C., Chiumenti M. On the numerical modeling of frictional wear phenomena. *Comput. Methods Appl. Mech. Engrg.* 1999; **177**:404–426.
23. Johansson L. Numerical simulation of contact pressure evolution in fretting. *Journal of Tribology* 1994; **116**:247–254.
24. Stromberg N. A Newton method for three-dimensional fretting problems. *IJSS* 1999; **36**:2075–2090.
25. Shillor M., Sofonea M., Touzani R. Quasistatic frictional contact and wear of a beam. *Dyn.Continu. Discrete. Impuls. Systems (DCDIS)* 2000; **8**:201–218.
26. Gu R. J., Kuttler K. L., Shillor M. Frictional Wear of a Thermoelastic Beam. *Journal of Mathematical Analysis and Applications* 2000; **242**:212–236.
27. Gu R. J., Shillor M. Thermal and wear analysis of an elastic beam in sliding contact. *IJSS* 2001; **38**:2323–2333.
28. Fisher N. J., Chow A. B., Weckwerth M. K. Experimental fretting wear studies of steam generator materials. *Journal of Pressure Vessel Technology* 1995; **117**:312.
29. Podra P. FE wear simulation of sliding contacts. *Doctoral Thesis, Royal Institute of Technology, Stockholm* 1997.
30. Eriksen M. The influence of die geometry on tool wear in deep drawing. *Wear* 1997; **207**:10–15.
31. Jourdan F. Numerical wear modeling in dynamics and large strains: Application to knee joint protheses. *Wear* 2006; **261**:283–292.
32. Podra P., Andersson S. Simulating sliding wear with finite element method. *Tribology International* 1999; **32**:71–81.
33. Podra P., Andersson S. Finite element analysis wear simulation of a conical spinning contact considering surface topography. *WEAR* 1999; **224**:13–21.
34. Oqvist M. Numerical simulations of mild wear using updated geometry with different step size approaches. *Wear* 2001; **249**:6–11.
35. Hyung-Kyu Kim, Seon-Jae Kim, Kyung-Ho Yoon, Heung-Seok Kang and Kee-Nam Song Fretting wear of laterally supported tube. *WEAR* 2001; **250**:535–543.
36. Lee C. Y. Theoretical analysis for studying the fretting wear problem of steam generator tubes in a nuclear power plant. *Nuclear engineering and technology* 2005; **37**:201-206.
37. Hyung-Kyu Kim, Young-Ho Lee Wear depth model for thin tubes with supports. *WEAR, In Press, Corrected Proof* 2007.
38. McColl I. R., Ding J., Leen S. B. Finite element simulation and experimental validation of fretting wear. *Wear* 2004; **256**:1114–1127.
39. Ding J., Leen S. B., McColl I. R. The effect of slip regime on fretting wear-induced stress evolution.

International Journal of Fatigue 2004; **26**:521–531.
40. Madge J. J., Leen S. B., Shipway P.H. The critical role of fretting wear in the analysis of fretting fatigue. *Wear, In Press, Corrected Proof* 2007.
41. Paulin C., Fouvry S., Meunier C. Finite element modelling of fretting wear surface evolution: Application to a Ti-6A1-4V contact. *Wear* 2007; **Early View**.
42. T. Belytschko, Y. Y. Lu and L. Gu Crack propagation by element-free Galerkin methods. *Engineering Fracture Mechanics* 2005; **194**:3022–3046.
43. Hyun-Gyu Kim Arbitrary placement of local meshes in a global mesh by the interface-element method (IEM). *International Journal for Numerical Methods in Engineering* 2003; **56**:2279–2312.
44. Haruhiko Kohno, Takahiko Tanahashi Numerical analysis of moving interfaces using a level set method coupled with adaptive mesh refinement. *International Journal for Numerical Methods in Engineering* 2004; **45**:921–944.
45. Prabel B., Combescure A., Gravouil A., Marie S. Level set X-FEM non-matching meshes: application to dynamic crack propagation in elastic-plastic media. *International Journal for Numerical Methods in Engineering* 2007; **69**:1553–1569
46. Young-Sam Cho, Sukky Jun, Seyoung Im, Hyun-Gyu Kim An improved interface element with variable nodes for non-matching finite element meshes. *Comput. Methods Appl. Mech. Engrg.* 2005; **194**:3022–3046.
47. Jae Hyuk Lim, Seyoung Im, Young-Sam Cho MLS (moving least squares)-based finite elements for three-dimensional nonmatching meshes and adaptive mesh refinement. *Comput. Methods Appl. Mech. Engrg.* 2007; **196**:2216–2228.
48. B. Nayroles, G. Touzot, P. Villon Generalizing the finite element method : diffuse approximation and diffuse elements. *Comput. Mech.* 1992; **10**:307–318.
49. P. Villon, H. Bourouchaki, K. Saanouni Transfert de champs plastiquement admissibles. *C. R. Mécanique* 2002; **330**:313–318.
50. T. Dick Modélisation multiéchelle du phénomène de fretting dans le contact aube-disque. *PhD Thesis, Centre des matériaux P. M. Fourt de lÉcole des Mines de Paris* 2006.
51. T. Liskiewicz, S. Fouvry, B. Wendler Development of a Wohler-like approach to quantify the Ti(C_xN_y) coatings durability under oscillating sliding conditions. *Wear* 2005; **259**:835–841.